Heads *and* Tails: Simultaneous Exposed and Buried Interface Imaging of Monolayers

Patrick Han,[†] Adam R. Kurland,[†] Andrea N. Giordano,[†] Sanjini U. Nanayakkara,[†,⊥] Meaghan M. Blake,[†] Chris M. Pochas,[†] and Paul S. Weiss[†,‡,§,*]

[†]Department of Chemistry, The Pennsylvania State University, University Park, Pennsylvania 16802, [‡]Department of Physics, The Pennsylvania State University, University Park, Pennsylvania 16802, and [§]California NanoSystems Institute and Department of Chemistry and Biochemistry, University of California, Los Angeles, California 90095. [⊥]Current address: Department of Materials Science & Engineering, University of Pennsylvania, Philadelphia, PA 19104.

ABSTRACT We have simultaneously imaged the chemically bound head groups and exposed tail groups in bicomponent alkanethiolate self-assembled monolayers on Au{111} with molecular resolution. This has enabled us to resolve the controversy of scanning tunneling microscopy image interpretation and to measure the molecular polar tilt and azimuthal angles. Our local measurements demonstrate that ordered domains with different superstructures also have varied buried sulfur head group structures.

KEYWORDS: scanning tunneling microscopy · self-assembled monolayers · barrier height · molecular tilt · sulfur–gold interface

Alkanethiolate self-assembled monolayers (SAMs) on Au{111} are the most studied synthetic self-assembled systems.[1−6] While the majority of recent work on SAMs has explored their applications in molecular electronics, nanofabrication, and biosensors,[4,5] key fundamental issues remain poorly understood. For example, the high-coverage self-assembly of simple linear alkanethiolate molecules on Au{111} surfaces involves a multitude of more complex stages such as lifting of the (22 × $\sqrt{3}$) Au reconstruction, upright molecular alignment at specific orientations, and formation of both the ($\sqrt{3}$ × $\sqrt{3}$)*R*30° and the *c*(4 × 2) superstructures in neighboring domains.[3] Questions such as what happens to the additional Au atoms after self-assembly,[6] and what leads to the existence of several superstructures for long-chain (number of carbon, $n \geq 6$) SAMs[7−9] remain subjects of intense research. Achieving fundamental understanding of how such complexity arises from such a simple system is a first step toward the ultimate goals of self-assembly, such as the synthesis of supramolecular functional systems whose complexity can rival biological systems.[10−12] Here, we present a technique that adds a third dimension to the sensitivity of scanning tunneling microscopy (STM) on SAMs, determining molecular tilt and azimuthal orientation. This technique will have important applications in more complex processes where changes in molecular tilt are important aspects of molecular function.[13,14]

Experimental investigations of the S−Au interface in SAMs have used ensemble techniques such as normal incidence X-ray standing waves (NIXSW)[9,15] and grazing incidence X-ray diffraction (GIXD).[7,16] The current consensus is that the S−Au interface involves some form of Au adatom-bound S species.[17,18] Strong evidence shows the presence of Au adatom−dithiolate species (two alkanethiolate molecules bound to a single Au adatom) for low-coverage short-chain ($n \leq 4$) SAMs.[16−18] However, the consensus breaks down for high-coverage systems, where observations from different X-ray techniques appear inconsistent. GIXD and density functional theory (DFT)-based simulations predict a single Au adatom−dithiolate structure in methylthiolate (**C1**) and hexanethiolate (**C6**) SAMs, for both the ($\sqrt{3}$ × $\sqrt{3}$)*R*30° and the *c*(4 × 2) domains.[7] This proposed structure contradicts NIXSW measurements for **C1**, butanethiolate (**C4**), **C6**, and octanethiolate (**C8**) SAMs, which suggest different S−Au lattice structures for the ($\sqrt{3}$ × $\sqrt{3}$)*R*30° and the *c*(4 × 2) domains, involving Au adatom−monothiolate species.[9,15]

One key issue that perpetuates this deadlock is the ensemble nature of the two X-ray techniques. Even though it is highly sensitive to the locations of the strongly scattering Au atoms, GIXD is ill-suited for investigating high-coverage

*Address correspondence to stm@ucla.edu.

Received for review August 18, 2009 and accepted September 14, 2009.

Published online September 22, 2009.
10.1021/nn901030x CCC: $40.75

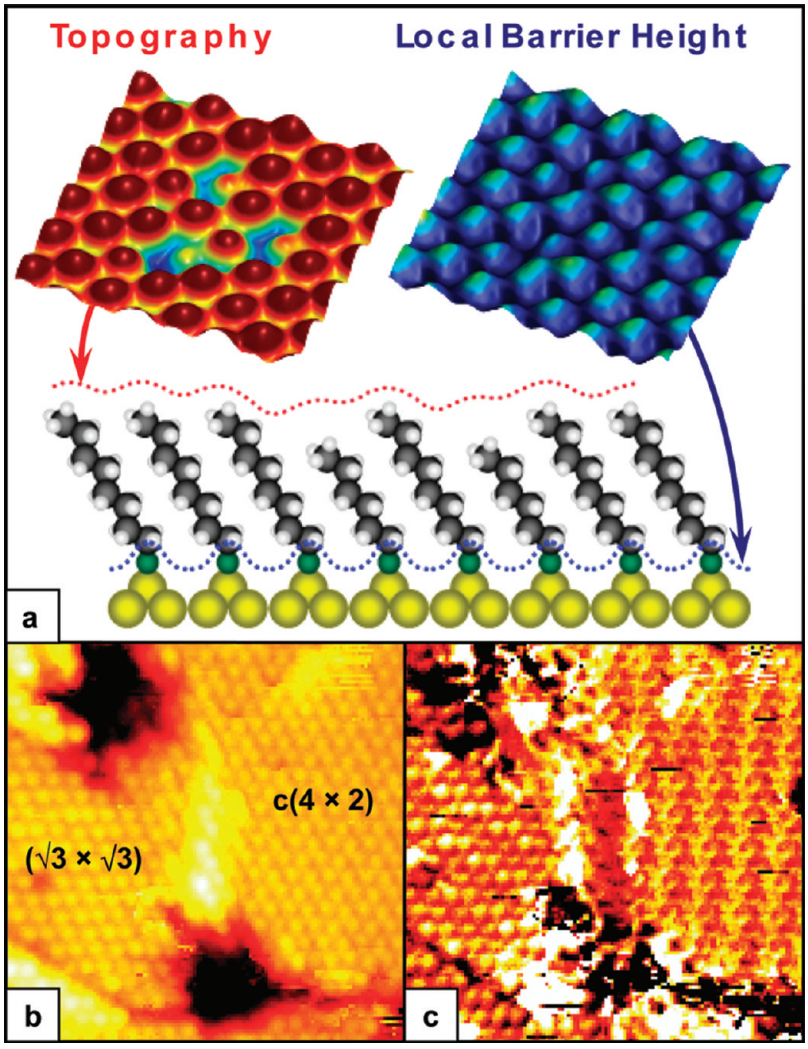

Figure 1. Experimental strategy: Simultaneous topography and barrier height imaging. (a) Schematic of the molecular orientation measurement. The top of panel a shows the simultaneously acquired topographic and LBH images of a C8/C6 bicomponent SAM (25 Å × 30 Å, V_s = 1.2 V, I_t = 11 pA). With this particular STM probe tip, topography measures the methyl termini, while LBH measures the S−Au interface of the alkanethiolate layer. (b) Topographic STM image (100 Å × 100 Å, V_s = −1.0 V, I_t = 15 pA) of a C12 SAM. The protruding feature at the center of the image is a domain boundary. Here, the *c*(4 × 2) domain can be distinguished by its herringbone pattern. (c) Barrier height STM image acquired simultaneously with panel b. The (√3 × √3)*R*30° domain shows a hexagonal pattern, while the *c*(4 × 2) domain shows a nonhexagonal pattern. The location of the thiolate head groups of the *c*(4 × 2) domain has not been determined.

long-chain ($n \geq 6$) SAMs, where the coexistence of the (√3 × √3)*R*30° and the *c*(4 × 2) domains is inevitable.[6] A single-molecule technique such as STM would be an ideal alternative, provided that we first resolve the controversy surrounding the interpretation of STM topographic images of SAMs. While STM can resolve the apparent height difference between alkanethiolate molecules of different lengths in a bicomponent SAM (assuming that the methyl termini are imaged),[19,20] conditions inducing disorder in the alkyl chains still yield periodic features (implying that the thiolate head groups are imaged).[21,22] Still other experimental results suggest that STM's sensitivity to either interface is also tip-dependent.[20,23] This ambiguity has prevented the direct study of the S−Au interface with STM.

In other STM experiments, we have been able to "peer through" a thin molecular overlayer to image substrate atoms and thereby to make absolute site assignments.[24,25] Here, we use a low-temperature (4 K) ultrastable STM[26] to image bicomponent SAMs. We first resolve the controversy of STM image interpretation by imaging simultaneously in constant-current topographic and in local barrier height (LBH) modes. We use *in situ* preparation to control the state of the STM tip, which images the methyl termini of the SAMs in topographic mode (as in ref 19), and the S−Au bond in LBH mode. This latter imaging mode measures the potential barrier of the tunneling gap between the STM tip and the substrate and is sensitive to the more electronegative atomic species on the surface.[27] We demonstrate this method's sensitivity to both the exposed and buried interfaces by measuring the molecular orientations of the bicomponent SAMs and compare our results with values previously obtained by infrared spectroscopy (IR)[28,29] and GIXD.[30] Our measurements show that for **C8** and decanethiolate (**C10**) SAMs domains presenting (√3 × √3)*R*30° superstructures have the same (√3 × √3)*R*30° S−Au lattice structure, whereas the *c*(4 × 2) overlayers have a more complex buried structure.

We fabricate three bicomponent SAMs (**C8**/**C6**, nonanethiolate (**C9**)/heptanethiolate (**C7**), and **C10**/**C8**, all with molar ratio $\chi = 0.9$ for the longer thiolate molecule) and single-component dodecanethiolate (**C12**) SAMs, all prepared according to previously described methods.[19] The presence of the shorter alkanethiolate species in the bicomponent SAMs introduces an important structural effect: due to the polar tilt in SAMs, the methyl termini of the shorter molecules are constrained to present lateral shifts relative to the methyl termini from the surrounding molecules (Figure 1a). This lateral shift enables us (1) to monitor the tip state to test if the topographic mode always images the methyl termini and (2) to assign the Au-bound S atoms detected by LBH to their corresponding methyl termini for the measurements of the molecular orientations.

We use a Pt/Ir STM probe tip cut under ambient conditions and prepared *in situ* by voltage pulses. Our optimum tip is one that can measure the apparent height difference of the methyl termini[19,20] and probe the Au-bound S—the more electronegative surface species. We distinguish the desired tip state by comparing the number of local maxima from the topographic and the LBH images. We use only tips that detect equal numbers of

topographic and LBH maxima (see Figure S1 in Supporting Information).

The perspective images in Figure 1a demonstrate the capabilities of such a tip on a $(\sqrt{3} \times \sqrt{3})R30°$ phase of a **C8**/**C6** SAM. The topographic image (top left of Figure 1a) shows not only the apparent height difference between the three **C6** molecules and the surrounding **C8** molecules but also the lateral shift of the **C6** topographic maxima, consistent with this modality imaging the top of the molecular layer.[19,20] The LBH image (top right of Figure 1a) shows no such lateral shift of the local maxima, but instead a *single* lattice for the two-dimensional crystalline domain, consistent with measuring the buried S−Au interface. This observation is consistent with recent NIXSW measurements on **C1** and **C4** SAMs, which detect univalent adsorption sites for the thiolate head groups.[15] The sensitivity of LBH imaging to the S−Au interface is demonstrated further in panels b and c in Figure 1, which show the topographic and LBH images acquired simultaneously over two adjacent domains of a single-component **C12** SAM, respectively. While a weak herringbone pattern is apparent in the rightmost domain in the topographic image in Figure 1b, indicating its $c(4 \times 2)$ superstructure, the LBH image in Figure 1c displays two dramatically different buried S−Au lattice structures between the two domains. This direct observation is consistent with the NIXSW-based prediction by Yu *et al.* that the $(\sqrt{3} \times \sqrt{3})R30°$ and the $c(4 \times 2)$ domains should have different S−Au lattice structures.[9] Figure 1c also confirms the hexagonal $(\sqrt{3} \times \sqrt{3})R30°$ structure of the thiolate head groups within the $(\sqrt{3} \times \sqrt{3})R30°$ domain.

To test if the lateral shifts of the topographic maxima exemplified in Figure 1a are due to molecular orientation, we locate areas over bicomponent SAMs that encompass different rotational domains (Figure 2a). We select areas with the $c(4 \times 2)$ superstructure—evident as the herringbone pattern—to highlight these domains. Figure 2a shows the topographic images of one such area over a **C9**/**C7** SAM. The herringbone patterns of the $c(4 \times 2)$ structure reveal a 60° rotation between the two domains, caused by the observed three-fold symmetry of SAMs on Au{111}. The topographic maxima shifts of the isolated **C7** molecules from each domain show corresponding directionality (insets of Figure 2a), consistent with the role of molecular orientation in the observed shifts. We test the validity of our molecular orientation measurements using this surface structural effect; we expect the relative azimuthal orientation angles measured between adjacent rotational domains to be multiples of 60°.

The coordinate system used to describe alkanethiolate orientations in SAMs is shown in Figure 2b, where θ and α denote the polar and azimuthal angles, respectively, and δ denotes the surface projection of the shift between the Au-bound S and the methyl terminus of a single alkanethiolate molecule. Since this method pinpoints the molecular extremities, in effect, we have a direct means of measuring δ, θ, and α for each molecule. An additional angle—the axial twist—is required for a complete description of the orientation. Because we measure only the molecular extremities, we do not address this quantity. For this same reason, at this point, we exclude areas with the $c(4 \times 2)$ superstructure from our orientation measurements since, in addition to the S−Au configuration,[7,9] this structure could involve different molecular twists, complicating data interpretation.[8] Another reason for excluding the $c(4 \times 2)$ domains from this measurement is that the topographic image contrast of these domains is highly sensitive to the tunneling gap conditions;[31] this affects our

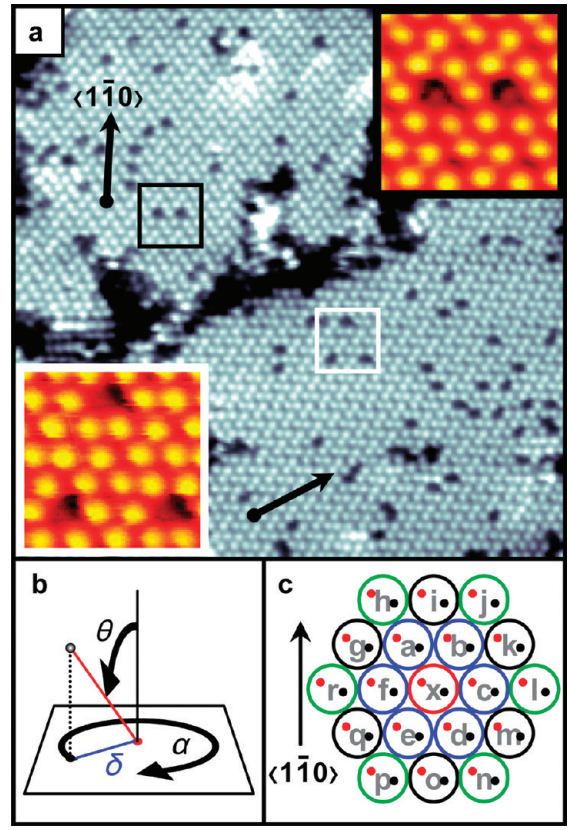

Figure 2. Effects of molecular tilt on local maxima imaged in the topographic mode. (a) Topographic STM image (270 Å × 270 Å, V_s = 1.2 V, I_t = 11 pA) showing two rotational $c(4 \times 2)$ domains of a C9/C7 bicomponent SAM. The insets (both 25 Å × 25 Å, V_s = 1.2 V, I_t = 11 pA) show the high-resolution STM images of the areas highlighted by the respective black and white squares. The different tilt directions are apparent when looking at the shorter C7 molecules. This effect is also observed on rotational domains of C8/C6 and C10/C8 bicomponent SAMs. The top black arrow shows the designated ⟨1$\bar{1}$0⟩ direction of the Au{111} substrate and the direction of the herringbone pattern. The bottom black arrow marks the 60° rotation of the bottom domain with respect to the ⟨1$\bar{1}$0⟩ direction. (b) Molecular orientation coordinate system. The θ and α represent the polar tilt angle and azimuthal angle, respectively. The δ denotes the surface projection of the shift between the S head group and methyl terminus of a single alkanethiolate molecule. (c) Coordinate system used to measure and bin δ values. Each black and red dot represents a topographic and LBH maximum, respectively. Letters a−r categorize the molecular azimuthal directions from x.

ability to locate local maxima consistently over $c(4 \times 2)$ domains.

In practice, each pair of topographic and LBH images yields two sets of local maxima. We assign the topographic local maxima to be the locations of the methyl termini (black dots in figures) and the LBH local maxima to be the locations of the thiolate head groups (red dots in figures). As exemplified by the black and red dots in Figure 2c, superimposing the two sets of local maxima does not straightforwardly reveal each thiolate's corresponding methyl terminus. The "head-to-tail" assignment of individual molecules is critical to our measurements and is discussed in detail below.

The colored circles in Figure 2c show the coordinate system used for measuring and binning the measured δ to make the molecular head-to-tail assignment. To measure the δ values of one alkanethiolate molecule, we anchor the red dot of the molecule of interest (red circle in Figure 2c) as the origin and measure every distance to the black dots of its nearest neighbor, next-nearest neighbor, and next-next-nearest neighbor locations (blue, black, and green circles, respectively in Figure 2c). This process is applied to every red dot of an image pair, and the resulting δ values are binned and averaged by direction according to the system shown in Figure 2c.

After acquiring topographic and LBH images simultaneously over two adjacent rotational domains of a **C8**/**C6** SAM, we use a digital image processing routine to select the local maxima (Figure S2 in Supporting Information). Because our experiment involves precise angular measurements, we rely on the stability of our instrument at 4 K to minimize thermal drift (a high-resolution 128 pixel $\times$ 128 pixel LBH image typically is acquired in $\sim$15 min). We correct any image aberration caused by residual drift and non-orthogonalities of the scanner tube (Figure S3 in Supporting Information). The resulting high-resolution topographic and LBH image pairs over two adjacent rotational domains of a **C8**/**C6** SAM with $(\sqrt{3} \times \sqrt{3})R30°$ superstructures are shown in Figure 3a–d.

Table 1 shows the measured δ, θ, and α values for the images in Figure 3a–d, averaged and listed according to the binning system in Figure 2c. To assign a topographic maximum to its corresponding LBH maximum, we assume that the molecular orientations of both the long and short alkanethiolate molecules within a single SAM domain must be nearly identical.

We use three criteria for our assignments: (1) the ratio δ_{C8}/δ_{C6} must be in close agreement with the ratio between the **C8** and **C6** molecular lengths (l_{C8}/l_{C6}); (2) both θ and α must be coherent between the corresponding **C8** and **C6**; and (3) the assignment must agree with the azimuthal orientation indicated by the maxima shift of the shorter alkanethiolate molecules in the topographic image. The total numbers of δ measurements used to compile Table 1 for each direction are given in Table S1 (Supporting Information).

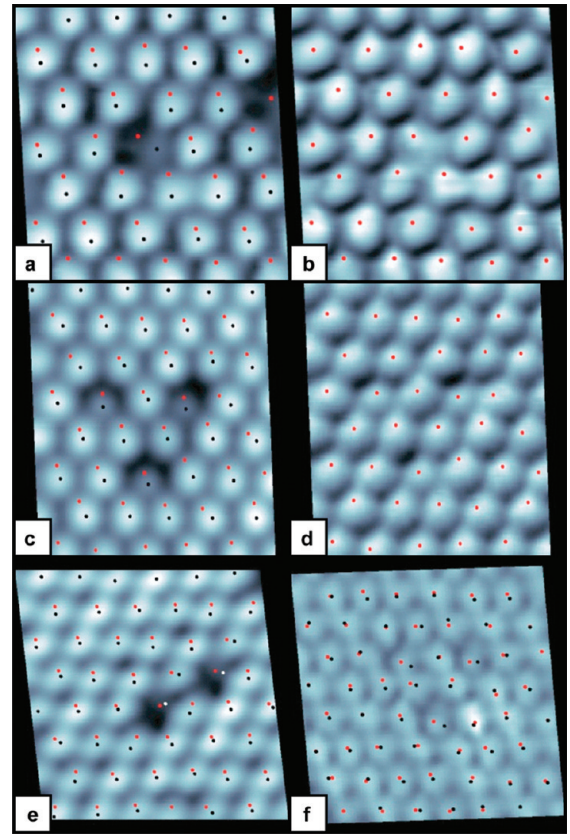

Figure 3. Alkanethiolate molecular extremities located and highlighted by digital image processing. (a) Topographic STM image (26 Å × 25 Å, V_s = 1.2 V, I_t = 11 pA) of a C8/C6 bicomponent SAM. (b) Barrier height STM image acquired simultaneously with image a. (c) Topographic STM image (25 Å × 30 Å, V_s = 1.2 V, I_t = 11 pA) of a rotational domain adjacent to image a. (d) Barrier height STM image acquired simultaneously with image c. Images a–d are acquired with the same scan direction. (e) Topographic STM image (35 Å × 34 Å, V_s = 1.2 V, I_t = 11 pA) of a C8/C6 bicomponent SAM, in an area that is macroscopically distant from a–d. (f) Barrier height STM image (35 Å × 30 Å, V_s = −1.2 V, I_t = 10 pA) of a C10/C8 bicomponent SAM. In images a, c, e, and f, the black and red dots show the locations of the simultaneously acquired topographic and LBH maxima, respectively. In images b and d, only the LBH maxima are shown. All areas in this figure are $(\sqrt{3} \times \sqrt{3})R30°$ domains.

From Figure 3a and the top half of Table 1, the directions b, g, and q present tilts with acceptable δ_{C8}/δ_{C6} and coherent θ and α values. We dismiss b for its θ of 16 $\pm$ 2°, which is not in agreement with the accepted range of $28° < \theta < 40°$.[28–30] While the topographic image of this data set does not allow us to choose unambiguously between the remaining two directions, we assign g to be the correct molecular orientation based on its better δ_{C8}/δ_{C6} agreement with l_{C8}/l_{C6} = 1.219.

Figure 3c and the bottom half of Table 1 show the measurements for a rotational domain adjacent to that in Figure 3a. Here again, while directions a and b are in good δ_{C8}/δ_{C6} agreement with l_{C8}/l_{C6}, we eliminate them for their small θ values. The best candidates with reasonable δ_{C8}/δ_{C6} are i and k.[32] We eliminate k for its α value, which does not agree with the azimuthal ori-

TABLE 1. Measured δ, α, and θ for Images Shown in Figure 3a,c[a]

Fig. 3a directions	δ_{C8} (Å)	δ_{C6} (Å)	δ_{C8}/δ_{C6} (I_{C8}/I_{C6} = 1.219)	α_{C8} (°)	α_{C6} (°)	θ_{C8} (°)	θ_{C6} (°)
a	3.4 ± 0.4	3.3	1.02	50 ± 9	54	14 ± 2	14
b	3.9 ± 0.4	3.3	1.19	44 ± 8	44	16 ± 2	14
c	5.6 ± 0.3	5.4	1.05	17 ± 4	26	24 ± 2	23
d	6.7 ± 0.4	6.4	1.04	64 ± 5	66	29 ± 2	27
e	6.4 ± 0.4	6.0	1.06	71 ± 5	73	27 ± 2	26
f	4.8 ± 0.6	5.3	0.92	19 ± 5	13	20 ± 3	22
g	7.6 ± 0.5	6.3	1.22	21 ± 4	26	33 ± 1	27
h	8.4 ± 0.5	8.8	0.95	56 ± 4	64	37 ± 2	39
i	6.9 ± 0.5	6.9	1.00	87 ± 3	83	30 ± 2	30
j	8.6 ± 0.5	10.0	0.86	53 ± 2	46	38 ± 3	46
k	8.1 ± 0.4	9.3	0.86	19 ± 4	16	35 ± 2	42
l	10.4 ± 0.5	11.5	0.90	13 ± 12	3	48 ± 3	56
m	9.7 ± 0.2	10.9	0.89	37 ± 3	33	44 ± 1	52
n	11.5 ± 0.4	11.1	1.03	61 ± 2	64	55 ± 3	53
o	10.1 ± 0.3	10.3	0.98	87 ± 2	82	47 ± 2	48
p	11.1 ± 0.4	10.3	1.08	66 ± 3	76	53 ± 3	48
q	9.2 ± 0.5	7.9	1.16	41 ± 2	42	41 ± 3	35
r	9.6 ± 0.5	9.4	1.02	9 ± 3	11	43 ± 3	42
Fig. 3c directions	δ_{C8} (Å)	δ_{C6} (Å)	δ_{C8}/δ_{C6} (I_{C8}/I_{C6} = 1.219)	α_{C8} (°)	α_{C6} (°)	θ_{C8} (°)	θ_{C6} (°)
a	3.7 ± 0.3	3.1 ± 0.1	1.23	59 ± 10	44 ± 8	16 ± 1	13 ± 1
b	4.3 ± 0.5	3.6 ± 0.2	1.22	44 ± 5	40 ± 4	18 ± 2	12 ± 1
c	5.7 ± 0.4	5.9 ± 0.5	0.98	14 ± 5	19 ± 3	24 ± 2	25 ± 3
d	6.5 ± 0.4	7.1 ± 0.3	0.91	61 ± 5	64 ± 7	28 ± 2	31 ± 2
e	5.9 ± 0.6	6.7 ± 0.7	0.89	72 ± 4	70 ± 6	25 ± 2	29 ± 4
f	4.6 ± 0.4	4.7 ± 0.5	0.97	16 ± 6	26 ± 7	19 ± 2	20 ± 3
g	7.6 ± 0.4	7.3 ± 0.4	1.04	24 ± 4	21 ± 3	33 ± 2	32 ± 3
h	8.7 ± 0.3	8.5 ± 0.4	1.03	59 ± 3	57 ± 2	39 ± 2	38 ± 3
i	7.4 ± 0.5	6.7 ± 0.7	1.11	86 ± 3	87 ± 2	32 ± 2	29 ± 3
j	9.2 ± 0.6	9.0 ± 0.6	1.02	54 ± 2	53 ± 3	41 ± 3	41 ± 5
k	8.6 ± 0.3	7.9 ± 0.4	1.09	21 ± 3	14 ± 1	38 ± 2	35 ± 3
l	10.6 ± 0.5	10.3 ± 0.7	1.03	8 ± 3	11 ± 1	50 ± 3	48 ± 8
m	9.9 ± 0.4	9.9 ± 0.3	1.00	35 ± 2	38 ± 1	45 ± 2	45 ± 3
n	11.3 ± 0.4	10.9 ± 0.7	1.03	61 ± 2	61 ± 3	54 ± 2	52 ± 4
o	10.0 ± 0.4	10.4 ± 0.2	0.96	86 ± 3	88 ± 1	46 ± 2	49 ± 3
p	10.8 ± 0.5	11.2 ± 0.4	0.97	66 ± 3	67 ± 1	51 ± 3	53 ± 4
q	8.8 ± 0.5	9.6 ± 0.2	0.92	39 ± 3	43 ± 2	39 ± 2	44 ± 1
r	8.8 ± 0.5	9.4 ± 0.1	0.99	8 ± 3	9 ± 4	44 ± 4	43 ± 1

[a]Each value is the average of every measurement in the same azimuthal direction according to the coordinate system in Figure 2c. The red boxes highlight the assigned molecular orientations. The standard deviations are shown where possible. Here, the α values are measured with respect to the horizontal direction.

entation found in Figure 3c. Therefore, we assign i as the only consistent direction of molecular orientation.

Our measurements over the two adjacent rotational domains show that alkanethiolates in both SAM regions have identical θ values within experimental error (33 ± 1 and 32 ± 2°). On the basis of the corresponding α values, the two rotational domains are measured to be out of phase by 65 ± 7°. This latter result is consistent with the 60° rotation observed in Figure 2a; we conclude that our technique indeed probes the exposed methyl termini and buried thiolate head groups simultaneously. With respect to the nearest Au $\langle 1\bar{1}0 \rangle$ directions (arrow in Figure 2c), the measured α values are 9 ± 4 and 4 ± 3° for the areas in Figure 3a,c, respectively.

We applied this method to measure the molecular orientation over relatively distant regions of a **C8**/**C6** SAM (Figure 3e), as well as a **C10**/**C8** SAM (Figure 3f). Table 2 compares the measured δ, θ, and α values for the areas in Figure 3a−f (full tables for Figure 3e,f are in Table S2 in Supporting Information). Our results indicate that, although significant variations in θ are observed over different regions of the same **C8**/**C6** SAM

TABLE 2. Comparisons of the Assigned Tilt Directions for Images Shown in Figure 3a−f[a]

Fig./Direction	δ_{C8} (Å)	δ_{C6} (Å)	δ_{C8}/δ_{C6} (I_{C8}/I_{C6}=1.219)	α_{C8} (°)	α_{C6} (°)	θ_{C8} (°)	θ_{C6} (°)
3a/g	7.6 ± 0.5	6.3	1.22	9 ± 4	4	33 ± 1	27
3c/i	7.4 ± 0.5	6.7 ± 0.7	1.11	4 ± 3	3 ± 2	32 ± 2	29 ± 3
3e/q	9.0 ± 0.5	7.7	1.17	5 ± 2	6	41 ± 3	43
Fig./Direction	δ_{C10} (Å)	δ_{C8} (Å)	δ_{C10}/δ_{C8} (I_{C10}/I_{C8}=1.180)	α_{C10} (°)	α_{C8} (°)	θ_{C10} (°)	θ_{C8} (°)
3f/i	8.5 ± 0.5	7.5 ± 0.8	1.13	5 ± 3	10 ± 7	31 ± 2	33 ± 4

[a]Here the α values are measured with respect to the nearest Au{111} $\langle 1\bar{1}0 \rangle$ direction. The standard deviations are shown where possible.

($\theta = 41 \pm 3°$ for Figure 3c), all polar tilt angles fall within the expected range.[28−30]

Measured azimuthal orientation angles over areas from different bicomponent SAMs show comparable values (all $\alpha \leq 10°$ with respect to the Au $\langle 1\bar{1}0 \rangle$ directions). This latter result seemingly contradicts the alkyl chain length dependence of α observed by GIXD, which predicts $\alpha_{\mathbf{C8}} > 15°$ with respect to the Au $\langle 1\bar{1}0 \rangle$ directions.[30] We note that both **C8** and **C10** are molecules with alkyl chain lengths in an intermediate regime where the energy balance between the intermolecular interactions and head group−substrate interactions is changing,[28] making the orientations of these molecules less predictable.[3] More statistically significant measurements are necessary to ascertain the specific orientations of these molecules.

This dual imaging mode technique measures molecular orientations by locating the extremities of alkanethiolate molecules within SAMs. We have also resolved the problem of STM image contrast assignment when imaging SAM systems. We tested the validity of this method by comparing local molecular orientation measurements with previous results observed by IR and GIXD.[28−30] These measurements show that for longer-chain high-coverage SAMs (**C8** and **C10**), domains presenting $(\sqrt{3} \times \sqrt{3})R30°$ superstructure have the same $(\sqrt{3} \times \sqrt{3})R30°$ S−Au lattice structure; the $c(4 \times 2)$ overlayers have more complex buried structures (Figure 1b,c), consistent with inferences from previous NIXSW observations.[9] While the STM probes the locations of the S atoms in the LBH mode, different tip states could be sensitive to the Au adatoms (Figure S1c,d in Supporting Information).

Other systems, such as the alkaneselenolates appear to have even more complicated buried interface structures, presumably due to the promiscuity of the Se−Au bonding.[33,34] The moiré patterns observed in the STM images of those systems are likely due to contributions from the effects described above. We anticipate that the measurements described here can be performed at room temperature and may help elucidate the complex interface bonding found in a number of SAMs as well as of molecules inserted into SAMs.[13,14]

Simultaneous imaging of the exposed and the buried interfaces adds a third dimension to the sensitivity of STM, extending it to measurements of greater complexity and insight.

METHODS

SAM Preparation. The chemicals *n*-hexanethiol, *n*-heptanethiol, *n*-octanethiol, *n*-nonanethiol, *n*-decanethiol, *n*-dodecanethiol (Sigma-Aldrich, St. Louis, MO), and 200-proof ethanol (Pharmco, Brookfield, CT) were used as received. The Au{111} on mica substrates (Agilent Technology, Tempe, AZ) was hydrogen-flame-annealed prior to SAM formation. Both the single- and the bicomponent SAMs were fabricated by immersing Au substrates into gravimetrically prepared 1 mM ethanolic solutions for 24 h at room temperature. For bicomponent SAMs, the ethanolic stock solutions of mixed *n*-alkanethiols were prepared such that the mole ratio of the longer molecule to the shorter molecule was 9:1, respectively. After the 24 h solution deposition, substrates were rinsed thoroughly with neat ethanol, dried under a stream of ultrahigh purity argon, and introduced into the UHV chamber.

STM Measurements. All STM measurements were carried out using a custom-built Besoke-style STM under cryogenic (4 K), extreme high vacuum ($<10^{-12}$ Torr) conditions. Both topographic and LBH images were acquired simultaneously in constant current mode with a current set point of 11 pA and a sample bias of +1.2 V. All LBH images were acquired by a small AC modulation of the tunneling gap distance (with amplitudes of 0.1−0.6 Å and frequencies of 3.0−3.5 kHz) and measuring the derivative of the modulated current signal using a lock-in amplifier (Stanford Research Systems SR850 DSP, Sunnyvale, CA).

Image Processing Routine for Orientation Measurements. All STM measurements were carried out using an automated digital image processing routine developed in Matlab R2008b (The MathWorks, Natick, MA) to remove high-frequency noise and intensity spikes that could have otherwise impaired the ability to pick maxima reliably (Figure S2 in Supporting Information). Because STM data are acquired by rastering (pixel by pixel), the overall dimensions of the image data are represented in pixel values. We implemented the matrixsmooth algorithm (for all code referred to here, see Figure S2 in Supporting Information) for manipulating raw data in the form of an $n \times n$ intensity map. The algorithm utilizes a nonweighted moving average with a user-defined sampling window. The smoothing function was applied line-by-line in the horizontal direction and repeated row-by-row in the vertical direction. Following smoothing, we implemented the algorithm, localMaximum, to find and index local maxima across the image matrix. The algorithm applies Matlab's imdilate function whose structuring element size is defined by the user as [q r] in the usage line. We have found that the threshold for reliable maxima picking occurs when $q,r \geq 2$. These procedures were repeated for each pair of simultaneously acquired topographic and LBH data, and the resulting maxima points were merged for measurement.

The image drift corrections were performed in Adobe Illustrator (Adobe Systems Incorporated, San Jose, CA). A step-by-step example of the drift correction is shown in Figure S3 in Supporting Information. The relevant distances between local maxima were also measured in Adobe Illustrator.

Acknowledgment. The authors gratefully acknowledge support from the Department of Energy, the National Science Foundation, and the Air Force Office of Scientific Research.

Supporting Information Available: Additional discussion and figures on STM tip preparation, digital data processing methods, and complementary measurements. This material is available free of charge *via* the Internet at http://pubs.acs.org.

REFERENCES AND NOTES

1. Nuzzo, R. G.; Allara, D. L. Adsorption of Bifunctional Organic Disulfides on Gold Surfaces. *J. Am. Chem. Soc.* **1983**, *105*, 4481–4483.
2. Ulman, A. Formation and Structure of Self-Assembled Monolayers. *Chem. Rev.* **1996**, *96*, 1533–1554.
3. Schreiber, F. Structure and Growth of Self-Assembling Monolayers. *Prog. Surf. Sci.* **2000**, *65*, 151–256.
4. Smith, R. K.; Lewis, P. A.; Weiss, P. S. Patterning Self-Assembled Monolayers. *Prog. Surf. Sci.* **2004**, *75*, 1–68.
5. Love, J. C.; Estroff, L. A.; Kriebel, J. K.; Nuzzo, R. G.; Whitesides, G. M. Self-Assembled Monolayers of Thiolates on Metals as a Form of Nanotechnology. *Chem. Rev.* **2005**, *105*, 1103–1169.

6. Woodruff, D. P. The Interface Structure of *n*-Alkylthiolate Self-Assembled Monolayers on Coinage Metal Surfaces. *Phys. Chem. Chem. Phys.* **2008**, *10*, 7211–7221.
7. Cossaro, A.; Mazzarello, R.; Rousseau, R.; Casalis, L.; Verdini, A.; Kohlmeyer, A.; Floreano, L.; Scandolo, S.; Morgante, A.; Klein, M. L.; *et al.* X-ray Diffraction and Computation Yield the Structure of Alkanethiols on Gold(111). *Science* **2008**, *321*, 943–946.
8. Delamarche, E.; Michel, B.; Gerber, C.; Anselmetti, D.; Guntherodt, H. J.; Wolf, H.; Ringsdorf, H. Real-Space Observation of Nanoscale Molecular Domains in Self-Assembled Monolayers. *Langmuir* **1994**, *10*, 2869–2871.
9. Yu, M.; Bovet, N.; Satterley, C. J.; Bengio, S.; Lovelock, K. R. J.; Milligan, P. K.; Jones, R. G.; Woodruff, D. P.; Dhanak, V. True Nature of an Archetypal Self-Assembly System: Mobile Au−Thiolate Species on Au(111). *Phys. Rev. Lett.* **2006**, *97*, 166102.
10. Philp, D.; Stoddart, J. F. Self-Assembly in Natural and Unnatural Systems. *Angew. Chem., Int. Ed. Engl.* **1996**, *35*, 1155–1196.
11. Whitesides, G. M.; Grzybowski, B. Self-Assembly at All Scales. *Science* **2002**, *295*, 2418–2421.
12. Weiss, P. S. Functional Molecules and Assemblies in Controlled Environments: Formation and Measurements. *Acc. Chem. Res.* **2008**, *41*, 1772–1781.
13. Donhauser, Z. J.; Mantooth, B. A.; Kelly, K. F.; Bumm, L. A.; Monnell, J. D.; Stapleton, J. J.; Price, D. W.; Rawlett, A. M.; Allara, D. L.; Tour, J. M.; *et al.* Conductance Switching in Single Molecules through Conformational Changes. *Science* **2001**, *292*, 2303–2307.
14. Moore, A. M.; Dameron, A. A.; Mantooth, B. A.; Smith, R. K.; Fuchs, D. J.; Ciszek, J. W.; Maya, F.; Yao, Y. X.; Tour, J. M.; Weiss, P. S. Molecular Engineering and Measurements to Test Hypothesized Mechanisms in Single Molecule Conductance Switching. *J. Am. Chem. Soc.* **2006**, *128*, 1959–1967.
15. Roper, M. G.; Skegg, M. P.; Fisher, C. J.; Lee, J. J.; Dhanak, V. R.; Woodruff, D. P.; Jones, R. G. Atop Adsorption Site of Sulphur Head Groups in Gold−Thiolate Self-Assembled Monolayers. *Chem. Phys. Lett.* **2004**, *389*, 87–91.
16. Mazzarello, R.; Cossaro, A.; Verdini, A.; Rousseau, R.; Casalis, L.; Danisman, M. F.; Floreano, L.; Scandolo, S.; Morgante, A.; Scoles, G. Structure of a CH_3S Monolayer on Au(111) Solved by the Interplay between Molecular Dynamics Calculations and Diffraction Measurements. *Phys. Rev. Lett.* **2007**, *98*, 016102.
17. Kautz, N. A.; Kandel, S. A. Alkanethiol/Au(111) Self-Assembled Monolayers Contain Gold Adatoms: Scanning Tunneling Microscopy before and after Reaction with Atomic Hydrogen. *J. Am. Chem. Soc.* **2008**, *130*, 6908–6909.
18. Maksymovych, P.; Sorescu, D. C.; Yates, J. T. Gold-Adatom-Mediated Bonding in Self-Assembled Short-Chain Alkanethiolate Species on the Au(111) Surface. *Phys. Rev. Lett.* **2006**, *97*, 146103.
19. Bumm, L. A.; Arnold, J. J.; Charles, L. F.; Dunbar, T. D.; Allara, D. L.; Weiss, P. S. Directed Self-Assembly to Create Molecular Terraces with Molecularly Sharp Boundaries in Organic Monolayers. *J. Am. Chem. Soc.* **1999**, *121*, 8017–8021.
20. Klein, H.; Battaglini, N.; Bellini, B.; Dumas, P. STM of Mixed Alkylthiol Self-Assembled Monolayers on Au(111). *Mater. Sci. Eng., C* **2002**, *19*, 279–283.
21. Widrig, C. A.; Alves, C. A.; Porter, M. D. Scanning Tunneling Microscopy of Ethanethiolate and Normal-Octadecanethiolate Monolayers Spontaneously Adsorbed at Gold Surfaces. *J. Am. Chem. Soc.* **1991**, *113*, 2805–2810.
22. Schönenberger, C.; Jorritsma, J.; Sondaghuethorst, J. A. M.; Fokkink, L. G. J. Domain-Structure of Self-Assembled Alkanethiol Monolayers on Gold. *J. Phys. Chem.* **1995**, *99*, 3259–3271.
23. Bucher, J. P.; Santesson, L.; Kern, K. Selective Imaging of Self-Assembled Monolayers by Tunneling Microscopy. *Appl. Phys. A: Mater. Sci. Process.* **1994**, *59*, 135–138.
24. Pascual, J. I.; Jackiw, J. J.; Kelly, K. F.; Conrad, H.; Rust, H. P.; Weiss, P. S. Local Electronic Structural Effects and Measurements on the Adsorption of Benzene on Ag(110). *Phys. Rev. B* **2000**, *62*, 12632–12635.
25. Han, P.; Mantooth, B. A.; Sykes, E. C. H.; Donhauser, Z. J.; Weiss, P. S. Benzene on Au{111} at 4 K: Monolayer Growth and Tip-Induced Molecular Cascades. *J. Am. Chem. Soc.* **2004**, *126*, 10787–10793.
26. Ferris, J. H.; Kushmerick, J. G.; Johnson, J. A.; Youngquist, M. G. Y.; Kessinger, R. B.; Kingsbury, H. F.; Weiss, P. S. Design, Operation, and Housing of an Ultrastable, Low Temperature, Ultrahigh Vacuum Scanning Tunneling Microscope. *Rev. Sci. Instrum.* **1998**, *69*, 2691–2695.
27. Marchon, B.; Bernhardt, P.; Bussell, M. E.; Somorjai, G. A.; Salmeron, M.; Siekhaus, W. Atomic Arrangement of Sulfur Adatoms on Mo(001) at Atmospheric-Pressure—A Scanning Tunneling Microscopy Study. *Phys. Rev. Lett.* **1988**, *60*, 1166–1169.
28. Porter, M. D.; Bright, T. B.; Allara, D. L.; Chidsey, C. E. D. Spontaneously Organized Molecular Assemblies. 4. Structural Characterization of Normal-Alkyl Thiol Monolayers on Gold by Optical Ellipsometry, Infrared-Spectroscopy, and Electrochemistry. *J. Am. Chem. Soc.* **1987**, *109*, 3559–3568.
29. Nuzzo, R. G.; Dubois, L. H.; Allara, D. L. Fundamental Studies of Microscopic Wetting on Organic-Surfaces. 1. Formation and Structural Characterization of a Self-Consistent Series of Polyfunctional Organic Monolayers. *J. Am. Chem. Soc.* **1990**, *112*, 558–569.
30. Fenter, P.; Eberhardt, A.; Liang, K. S.; Eisenberger, P. Epitaxy and Chainlength Dependent Strain in Self-Assembled Monolayers. *J. Chem. Phys.* **1997**, *106*, 1600–1608.
31. Riposan, A.; Liu, G. Y. Significance of Local Density of States in the Scanning Tunneling Microscopy Imaging of Alkanethiol Self-Assembled Monolayers. *J. Phys. Chem. B* **2006**, *110*, 23926–23937.
32. While direction g in Figure 3a shows very good agreement between δ_{C8}/δ_{C6} and I_{C8}/I_{C6}, directions i and k in Figure 3b show a larger δ_{C8}/δ_{C6} deviation from I_{C8}/I_{C6}. We believe this is caused by a slight thermal drift during the data acquisition of Figure 3b, in the direction parallel to the tilt direction. This is evident from the vertical stretch of the figure. In effect, this thermal drift caused some data loss for our tilt measurement.
33. Monnell, J. D.; Stapleton, J. J.; Jackiw, J. J.; Dunbar, T.; Reinerth, W. A.; Dirk, S. M.; Tour, J. M.; Allara, D. L.; Weiss, P. S. Ordered Local Domain Structures of Decaneselenolate and Dodecaneselenolate Monolayers on Au{111}. *J. Phys. Chem. B* **2004**, *108*, 9834–9841.
34. Monnell, J. D.; Stapleton, J. J.; Dirk, S. M.; Reinerth, W. A.; Tour, J. M.; Allara, D. L.; Weiss, P. S. Relative Conductances of Alkaneselenolate and Alkanethiolate Monolayers on Au{111}. *J. Phys. Chem. B* **2005**, *109*, 20343–20349.